Effect of design parameters on thermal performance of integrated phase change material blind system for double skin façade buildings

Yilin Li[1]*, Jo Darkwa[2], Georgios Kokogiannakis[3] and Weiguang Su[4]
[1]*School of Environment and Architecture, University of Shanghai for Science and Technology, 516 Jungong Road, Shanghai 200093, China;* [2]*Faculty of Engineering, The University of Nottingham, University Park, Nottingham NG7 2RD, UK;* [3]*School of Mechanical, Materials and Mechatronic Engineering, Sustainable Building Research Centre, University of Wollongong, Innovation Campus, Fairy Meadow, NSW 2519, Australia;* [4]*School of Mechanical & Automotive Engineering, Qilu University of Technology (Shandong Academy of Sciences), Jinan 250353, China*

Abstract

Double skin facades (DSFs) have overheating problems in warm seasons which may increase the cooling loads in buildings. A previous study has developed an integrated phase change material (PCM) blind system and proved its capacity of mitigating the overheating phenomenon in DSFs. This paper focuses on the effect of design parameters on the thermal performance of such systems by conducting a simulation study of a DSF integrated with a PCM blind with different material properties, positions in cavity, and tilt angles of blades. The results indicate that the performance of the integrated PCM blind system can be optimised with careful geometric design and proper thermophysical properties of the PCM.

Keywords: double skin facade; PCM blind system; CFD

*Corresponding author: yilin.li@usst.edu.cn

Received 8 October 2018; revised 4 December 2018; editorial decision 14 January 2019; accepted 20 January 2019

1 INTRODUCTION

The building sector has been identified as one of the main contributors to energy consumption representing ~40% of the total world annual energy consumption [1]. For instance, in 2013, the building sector accounted for ~40.2% of total annual energy consumption in the United States of America [2]. Similarly in China, energy consumption in the building sector has increased by 40% over the past two decades mainly driven by population and economic growth, and projects to account for about 35% of total national energy consumption by 2020 [3]. In order to minimise this level of energy consumption in the building sector, significant efforts have been made in the development and utilisation of various sustainable building designs [4, 5]. Amongst them are double skin façades (DSFs) which have already become common architectural design features for their potential in saving energy in buildings [6–8].

Previous studies have shown that the DSFs could perform thermally better and reduce energy consumption in buildings than some conventional curtain wall structures during both winter and summer periods. For instance, Høseggen *et al.* [9] evaluated the energy performance of a DSF building against conventional single skin façade (SSF) building and found 20% heating energy reduction can be achieved in winter. Saber *et al.* [10] indicated that the DSF at different orientations can lower the air temperature and reduce cooling energy consumption in buildings. Studies by Rovers *et al.* [11] and Jun *et al.* [12] also support the fact that DSFs are capable of reducing energy consumption in buildings through the benefits of thermal buffer and natural ventilation.

International Journal of Low-Carbon Technologies 2019, 1–8

doi:10.1093/ijlct/ctz010

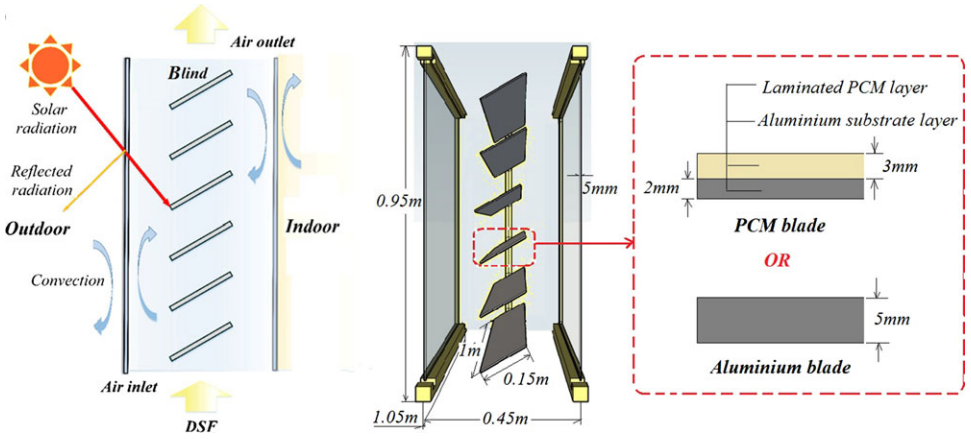

Figure 1. *Scheme of DSF integrated with the PCM blind system [25].*

This study mainly focused on the hot summer and cold winter regions in China where DSFs are preferred in winter and mid-season, but have severe overheating problem in summer which may cause unpleasant indoor environments and increased cooling loads in buildings [13–15]. The main causes of overheating in DSF include ineffective removal of heat stored within the DSF system, inappropriate location and size of shading devices, and inadequate operations of the DSF for specific thermal environmental conditions (such as lack of control for states of DSF openings or mechanical fans according to different weathers and seasons) [16]. To this end, some strategies have been adopted in DSF systems as solutions to overheating effect such as physical considerations at the design stage of DSFs [17, 18], and more flexible methods including utilisation of shading devices [19], integration of thermal mass [20] and application of energy storage materials such as phase change materials (PCMs) [21].

However, the venetian blind systems have the problem of high surface temperature and large secondary transmittance which may contribute to overheating in the adjacent space [22]. Thermal mass has limitations such as comparably low energy storage capacity and sacrifice of natural illumination [19]. De Gracia *et al.* [23] found that the overheating effect can be eliminated by including PCM in a DSF system. However, the PCM-DSF system needs to be optimised for overcoming the limitations of conventional venetian blinds and thermal mass systems, while achieving a certain level of natural illumination and flexible operation under various weather conditions. Weinlaeder *et al.* [24] monitored a solar blind system with macro-encapsulated PCM panels in a building and achieved some level of temperature reduction in comparison with a conventional blind. However, the systems suffered from low energy storage efficiency and solidification issues.

Although our previous research [25] has developed an integrated blind system for DSF by using micro-encapsulated PCM, there is still a lack of comprehensive studies on the performance of such PCM blind systems with different material and geometric properties. In this regard, this study investigates the impacts of different locations of the blind, blind tilt angles, and types of PCMs on the performance of the integrated PCM blind system for the purpose of optimisation of the system.

2 METHODOLOGY

2.1 System description and experimental set-up

A multilayer blind structure consisting of laminated composite PCM blades has been proposed based on our previous study (Figure 1(c)) [25, 26]. The PCM layer is intended to absorb any excess solar heat through the external glass skin which may be trapped in the DSF cavity, and in this way prevents additional heat gain into the adjacent indoor area. When the temperature in the cavity drops below the PCM solidification temperature, the stored heat is then discharged and removed by means of natural or mechanical ventilation.

For the purpose of validating the numerical models, a scale model test facility measured at 1.05 m × 0.95 m × 0.45 m was installed on the third floor of an existing multi-storey DSF building located at the Centre for Sustainable Energy Technologies (CSET), at University of Nottingham Ningbo, China. The laminated composite PCM blades were developed by using Rubitherm Company's micro-encapsulated PCM PX35. There were six blades in the box at a tilt angle of 30° south facing. Twenty K-type thermocouples were installed in the test rig for measuring the surface temperature of the blades, the surface temperature of the glass walls, and air temperature at different positions in the box. Two hotwire anemometers were employed to record the inlet and outlet airflow velocity in the DSF box. All the sensors were calibrated before installation and were connected to a data logging system set up in an office of CSET building for continuous data acquisition. The calibration shows that the errors from all the thermocouples were below 3% which was acceptable in this study. Except for some weekends and rainy days, the data collection was conducted continuously during the summer period and the time step of the data collection was 5 s. Meteorological data including

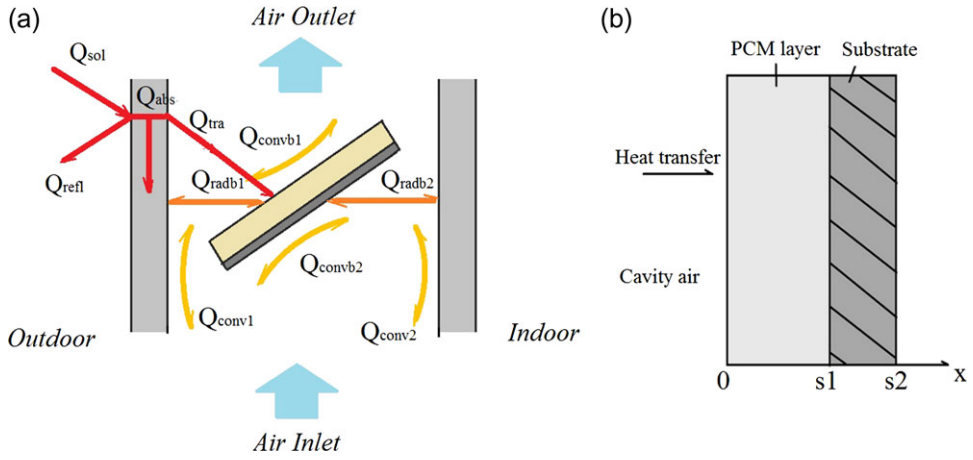

Figure 2. *DSF test facility integrated with the PCM blind system [25]. (**a**) Integrated DSF system, (**b**) sectional view of a PCM blade.*

ambient temperature, solar radiation, and wind speed and direction were monitored and recorded by a weather station located in front of the DSF at the CSET building. The measured data were used for defining the boundary conditions and for empirical evaluation of the system's performance.

2.2 Numerical models and simulation set-up

Figure 2 shows the heat transfer pathways in the DSF integrated with the PCM blind system. Numerical models were developed in our previous study [25] with the following assumptions and main equations:

- Both convective and radiative heat transfer exist on the surface of the PCM blind.
- Only one-dimensional conduction is considered within each PCM blade and convective heat transfer is negligible.
- The PCM is homogeneous and isotropic with constant thermophysical properties except its enthalpy.
- The thermophysical properties of the aluminium substrate are constant.
- There is no transmitted solar radiation on the internal glass skin of the DSF due to the length of the blade and the tilt angle of the blind.
- The airflow is treated as two-dimensional incompressible flow with constant air density.

The net solar heat gain (Q_{net}) and the total solar heat gain (Q_{sol}) into the DSF system can be calculated as Eq. (1) and Eq. (2).

$$Q_{\text{net}} = Q_{sol} - Q_{refl} - Q_{conv\_o} - Q_{conv\_i} \quad (1)$$

$$Q_{sol} = Q_{abs} + Q_{tra} + Q_{refl} \quad (2)$$

The heat conduction and energy equation within the PCM layer can be expressed as

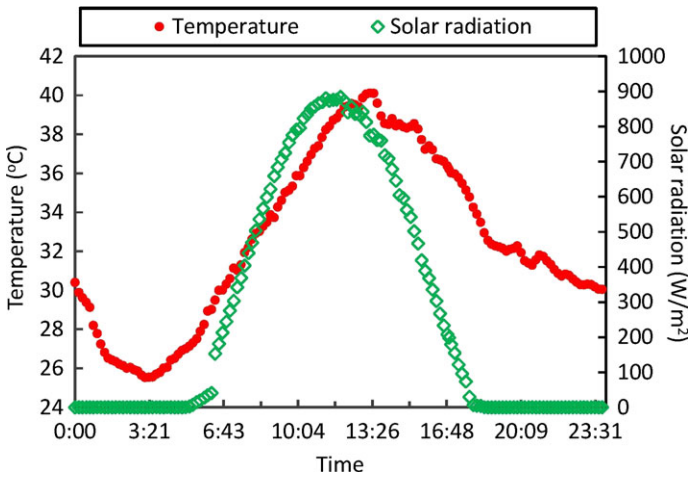

Figure 3. *Weather data for the simulation cases.*

Table 1. *Simulation cases.*

Case	Angle (°)	Position	Type of material
Case 0	30	Middle	Aluminium
Case 1	30	Middle	PCM1
Case 2	45	Middle	PCM1
Case 3	60	Middle	PCM1
Case 4	30	Close to external glass	PCM1
Case 5	30	Close to internal glass	PCM1
Case 6	30	Middle	PCM2

$$Q_b = k_p \left.\frac{dT_p}{dx}\right|_{0<x<s_1} \quad (3)$$

$$\left.\frac{\partial}{\partial t}(\rho_p H)\right|_{t>0} = k_p \left.\frac{\partial^2 T_p}{\partial x^2}\right|_{0<x<s1} \quad (4)$$

Table 2. *Physical properties of the system.*

Material	Density (kg/m^3)	Heat storage capacity (kJ/kg)	Melting temperature (°C)	Thermal conductivity (W/m K)	Reflectivity	Emissivity		Refractive index	Absorptivity
						External	Internal		
Glass	2500	—	—	1.1	0.16	0.84	0.84	1.5	0.15
Aluminium	2719	—	—	202.4	0.67	0.7	0.7	1.44	0.18
PCM1 (PX35)	650	100	29-36	0.1	0.52	0.9	0.9	—	0.8
PCM2 (RT25HC)	825	230	22-26	0.2	0.52	0.9	0.9	—	0.8

where

$$H = h + \Delta H \tag{5}$$

$$h = h_{ref} + \int_{T_{ref}}^{T} c_{Pp} dT \tag{6}$$

The heat conducted from the PCM layer to the substrate on the interface *s*1 can be calculated as:

$$k_p \frac{dT_p}{dx}\bigg|_{x=s_1} = k_s \frac{dT_s}{dx}\bigg|_{x=s_1} \tag{7}$$

The energy equation within the substrate is

$$\rho_s c_{Ps} \frac{\partial T_s}{\partial t}\bigg|_{t>0} = k_s \frac{\partial^2 T_s}{\partial x^2}\bigg|_{s_1<x<s_2} \tag{8}$$

The heat transferred to interface *s*2 of the substrate can be calculated as

$$Q_s = k_s \frac{dT_s}{dx}\bigg|_{x=s2} = Q_{rad\_b2} + Q_{conv\_b2} \tag{9}$$

The total heat transfer from the cavity air can be expressed as

$$Q_a = C_{Pa} m_a \Delta T_a = Q_{conv\_1} + Q_{conv\_2} + Q_{conv\_b1} + Q_{conv\_b2} \tag{10}$$

The general governing equations for the fluid domain are developed by using Navier–Stokes equations while the buoyancy effect of air is simulated with Boussinesq approximation. The general governing equations can be written as

$$\frac{\partial(\rho\varphi)}{\partial t} + \nabla(\rho\vec{U}\varphi) = \nabla(\Gamma_\varphi gra\varphi) + S_\varphi \tag{11}$$

where

$$\rho = \rho_0(1 - \alpha\Delta T) \tag{12}$$

ANSYS FLUENT software 14.5 was used for simulating the temperature and airflow distributions in the integrated DSF system. RNG k-ε model was selected as the turbulence model and discrete ordinates (DO) model was applied as the radiation model. The boundary conditions were set up based on the ambient temperature and solar radiation data in July – the hottest month during the summer as shown in Figure 3. The velocity inlet for DSF inlet at the bottom, pressure outlet for DSF outlet at the top, and walls with no slip boundary conditions for the DSF glass skins and blind surface. The dynamic boundary conditions were set up. For the solver solutions, SIMPLE scheme was selected as the pressure–velocity coupling method while second-order approximations were used as differential equations solutions.

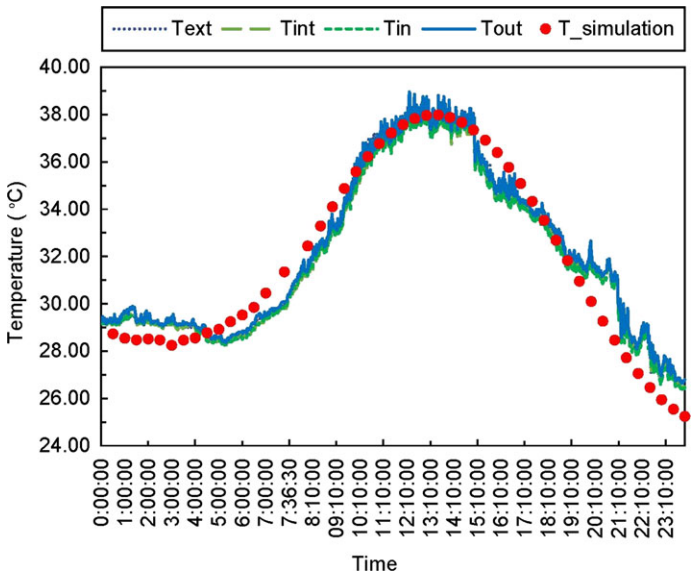

Figure 4. *Comparison of simulated and measured DSF air temperatures-Case 1 (Tin: inlet air temperature; Tout: outlet air temperature; Tint: air temperature near internal glass skin; Text: air temperature near external glass skin; T_simulated: simulated average air temperature).*

The cases simulated are presented in Table 1 and the physical properties of the material in the integrated systems are shown in Table 2. Three blind tilt angles were considered in Case 1 (30°), Case 2 (45°) and Case 3 (60°), while three different positions in DSF cavity were simulated in Case 1(Middle), Case 4 (Close to external glass) and Case 5 (Close to internal glass). In order to identify the influence of PCM thermal properties on the integrated system, the simulations and comparisons included PCM1 (Case 5: PX35) which is suitable for warm climatic regions and PCM2 (Case 6: RT25HC) which has a lower melting temperature

that is often suitable for mild climate regions. Case 0 consisting of aluminium blade without a PCM layer was also simulated for comparison purposes.

3 RESULTS AND VALIDATION

In order to validate the numerical models, simulation Case 1 with PCM blind in the middle of the cavity and tilt angle of 30° was regarded as a base case. The simulated average cavity air temperature of Case 1 has been compared against experimental data as shown in Figure 4. In general, it was found that the predicted average air temperature agreed reasonably well with the measured data.

The results of Case 1 show that the largest air temperature in DSF during a day occurred at 13:00 of the daytime when the ambient temperature was the highest. Figure 5 presents the surface temperatures of the PCM and aluminium blinds at different positions in DSF, and the differences between the simulated and measured data. It was found that the differences between simulated and measured data were lower than 4% and the average difference was 1.31%, which also demonstrates a good accuracy of the simulation results and proved the reliability of the numerical models.

This paper focused on the comparison of different simulation cases in a simulation cycle. Figure 6 shows the surface temperature on the sunny side and heat flux profiles of the blind systems with different blind tilt angles with PCM1. Among these cases, the surface temperature of aluminium blind in Case 0 was obviously higher than those of PCM blinds in other cases. The heat flux profiles indicate that the PCM blinds can absorb heat from the air cavity while the aluminium blind release heat to DSF cavity during the simulation. The heat flux for the aluminium blind was almost constant due to that there was little change in the temperature difference between the sunny side and the shaded side throughout the day. Other than Case 0, all the temperature and the heat flux profiles follow similar trends. For the temperature curves, the system in Case 2 (DSF with blind tilt angle of 45°) had the highest peak temperature, while the corresponding heat flux profile shows the lowest heat absorption ability. On the other hand, Case 1 (DSF with blind tilt angle of 30°) shows the highest heat absorption ability with the lowest negative heat flux. This is because that the blind tilt angle of 30° matches better the local latitude (N 28°51'–30°33') which enables the PCM blind to receive more of the solar radiation than the other cases. In the meanwhile, the surface temperature of the system in Case 2 was higher than that in Case 3 because of the higher amount of

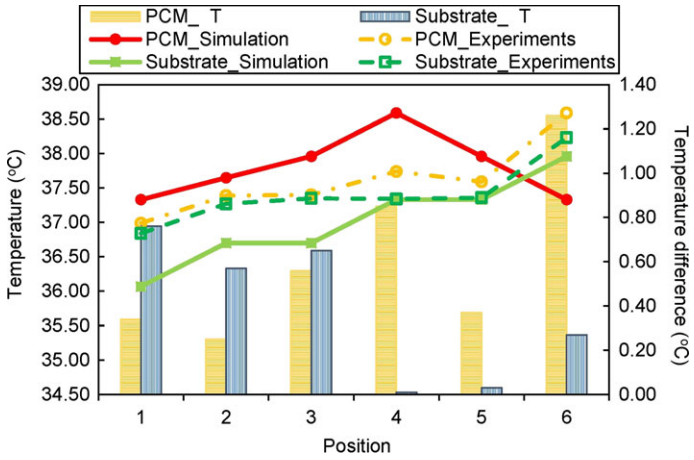

Figure 5. *Comparison of simulated and measured blind surface temperatures-Case 1 (PCM_ΔT/Substrate_ΔT: temperature difference between simulated and experimental data of PCM layer/substrate; PCM_Simulation/Substrate_Simulation: simulated temperature data of PCM layer/substrate; PCM_Experiments/Substrate_Experiments: experimental temperature data of PCM layer/substrate).*

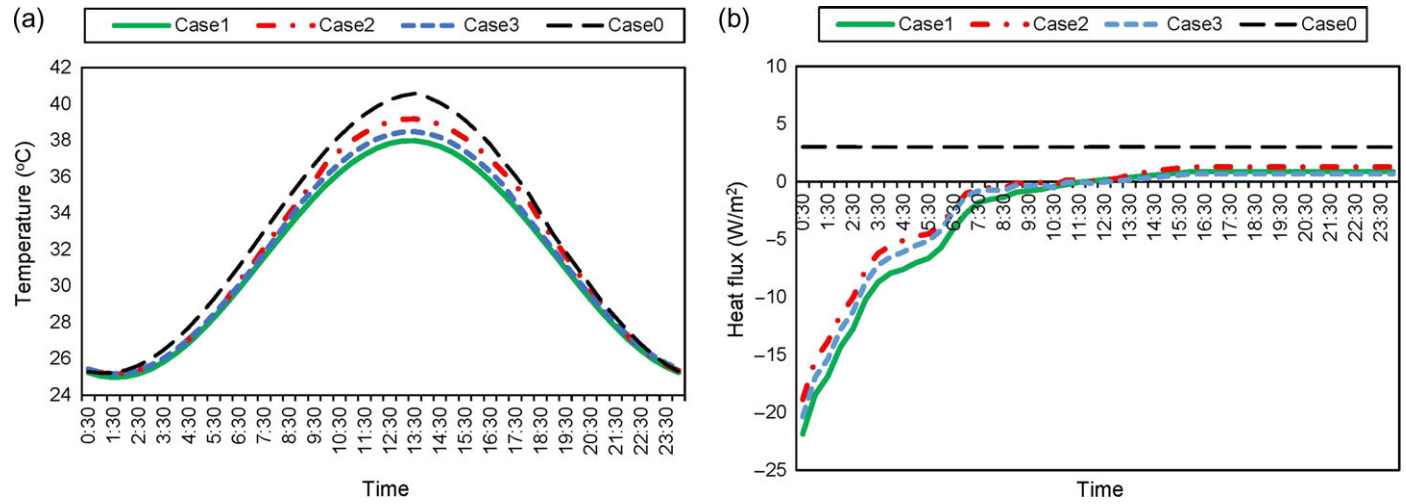

Figure 6. *Profiles of system with different blind tilt angles. (**a**) Temperature profile, (**b**) heat flux profile.*

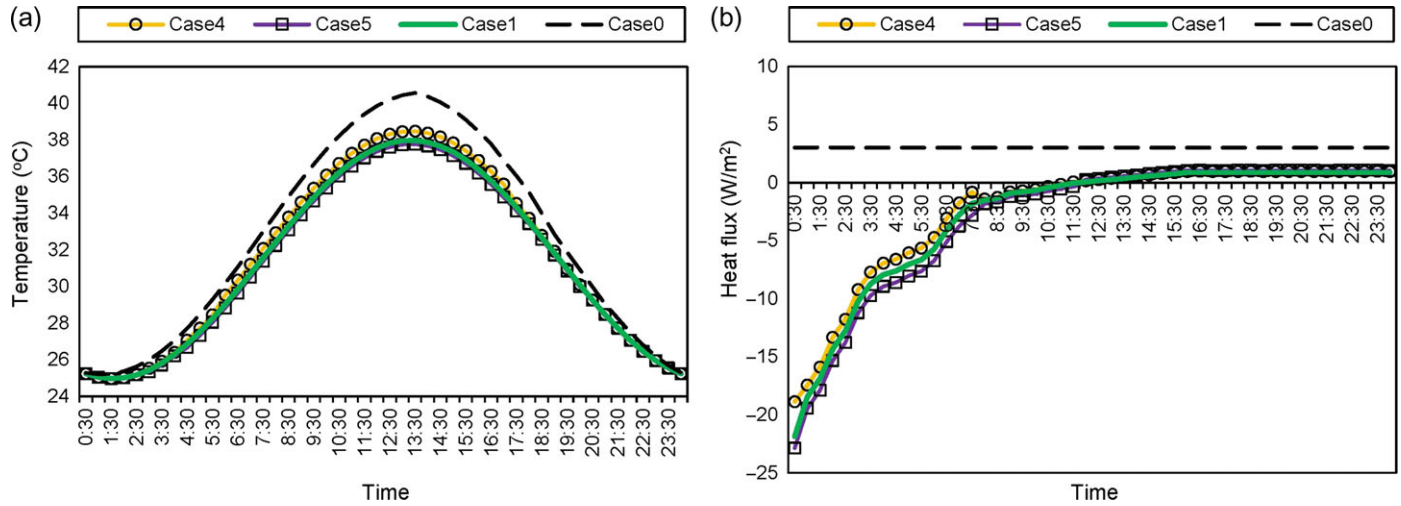

Figure 7. *Profiles of system with different positions in DSF. (**a**) Temperature profile, (**b**) heat flux profile.*

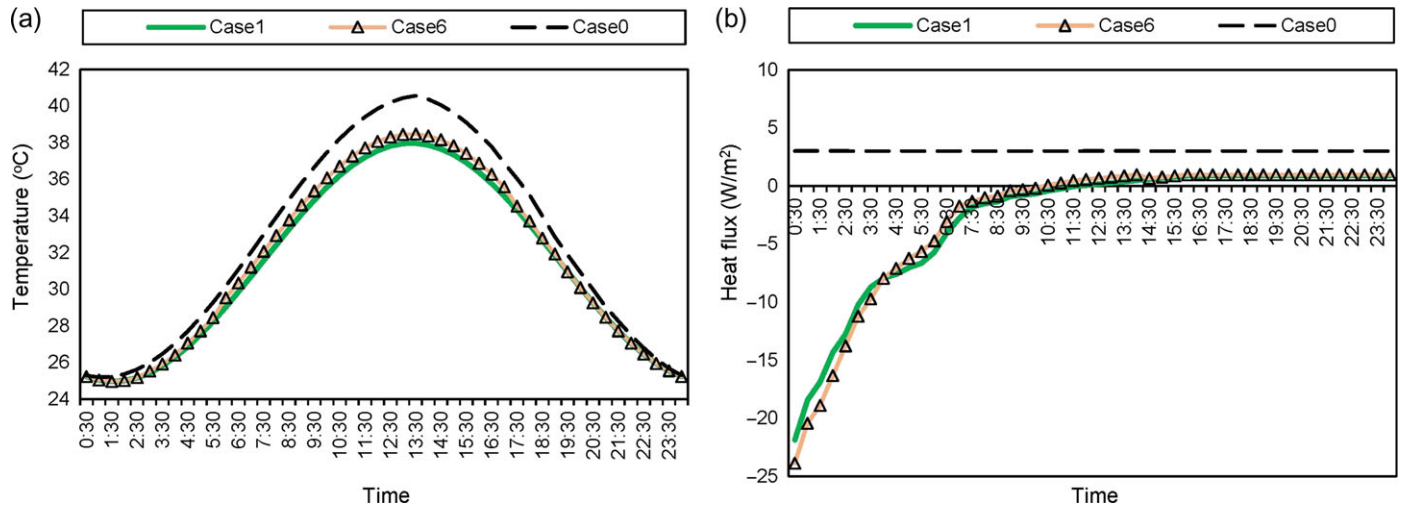

Figure 8. *Profiles of system with different PCMs. (**a**) Temperature profile, (**b**) heat flux profile.*

incidence solar radiation in Case 2 and possibly because the tilt angle of blind system in Case 3 results in larger vertical airflow velocity (average outlet vertical airflow velocity for Case 2 was 0.50 m/s while for Case 3 was 0.52 m/s) in the cavity and higher convective heat transfer on the surface.

Figure 7 demonstrates the surface temperature on the sunny side and heat flux profiles of systems with different blind positions in the DSF. Similar to Figure 6, the aluminium blind shows the highest temperature and no ability of heat absorption compared with the PCM blind cases. Except for Case 0, all the other temperature profiles and heat flux profiles follow similar trends. The temperature profile for Case 4 (blind close to external glass skin) was above the others and the temperature profile of Case 5 (blind close to internal glass skin) was the lowest. This was mainly due to the higher glass skin temperature of the external glass skin compared with the internal glass skin. The higher surface air temperature and thinner surface air layer influenced the convective heat transfer on the surface of the integrated blind system. Accordingly, the heat flux profile of Case 4 shows the lowest heat absorption ability among these cases while Case 5 shows the highest ability. Although the results show that the thermal performance of a system with the integrated blind close to the internal glass skin was the optimal amongst the cases studied, the distance between the integrated PCM blind and the two glass skins should be studied carefully in order to identify the proper position for installing the blind system.

Figure 8 presents the surface temperature on the sunny side and heat flux profiles of systems with different types of PCMs. Among these cases, the aluminium blind also shows the highest temperature and no heat-absorption ability. It can be seen that other than Case 0, there was almost no difference between the temperature profiles in Case 6 and Case 1 although the systems have different thermophysical properties. The actual heat absorption ability of the integrated blind system in Case 6 was a little bit higher than that in Case 5, even though the heat storage capacity and thermal conductivity of PCM2 in Case 6 were

larger than PCM1 in Case 5. This is due to that the highest cavity air temperature during the daytime was higher than but more close to the melting temperature of Case 5 compared with the melting temperature of Case 6.

4 CONCLUSION

A numerical study on an integrated PCM blind system in DSF was carried out in order to identify the effect of different design parameters and thus optimise the thermal performance of the system. The specific conclusions can be summarised as follows:

- The temperature and heat flux profiles of systems with different blind tilt angles follow similar trends respectively. Due to that the tilt angle matches better the local latitude, the temperature of the system with blind tilt angle of 30° was the lowest and the corresponding heat flux profile shows the highest heat absorption ability.
- The temperature and heat flux profiles of systems with different positions in DSF also follow similar trends respectively. The air temperature in DSF with blind close to the external glass skin was the highest, while the air temperature in DSF with blind close to the internal glass skin was the lowest. The distance between the integrated PCM blind and the two glass skins of the DSF should be studied further to define the proper position to install the blind system.
- There was no significant difference between the air temperature in DSFs with the two types of PCMs in this study due to that the cavity air temperature during the daytime was much higher than the melting temperature of PCM2 in Case 6. Therefore, careful decisions must be made when selecting PCM to include factors of both optimal energy storage capacity and melting temperature range suitable to the local environment.

Despite the above findings, the limitations of this study include a lack of detailed discussions on the impact of ambient environmental conditions (such as the air temperature, solar radiation and wind velocity) on the system. The effectiveness of the integrated system should be tested under various climatic and weather conditions for wider applications. Besides, there is the need for longer-term investigations into the energy storage efficiency of the PCM due to repeated charging and discharging cycles. Life cycle assessment of the developed integrated PCM blind system should also be conducted for achieving full technical and economic evaluation.

NOMENCLATURE

C_p	specific heat (kJ/kg K)
Q	heat (W)
H	enthalpy (kJ/kg)
ΔH	latent heat (kJ/kg)
T	temperature (K)
ΔT	temperature difference (K)
T_s	temperature on surface (K)
Φ	general variables
S_φ	source term (kg/m^3·s, N/m^3, W/m^3)
Γ_φ	diffusion coefficient (m^2/s)
$\overrightarrow{U}$	velocity vector (m/s)
h	convective heat transfer coefficient (W/m^{2}K)/sensible enthalpy (kJ/kg)
k	thermal conductivity (W/mK)
t	time (s)
ρ	density (kg/m^3)
net	net heat gain of DSF
sol	total solar radiation on the DSF
refl	reflected solar radiation
abs	absorbed solar radiation
tra	transmitted solar radiation
conv	convective heat transfer
rad	radiative heat transfer
a	cavity air
b	blind
k	turbulence kinetic energy
p	PCM layer of the blind
s	substrate of the blind

REFERENCES

[1] Omer AM. Green energies and the environment. *Renew Sust Energ Rev* 2008;**12**:1789–1821.

[2] U. S. Energy Information Administration. Energy Consumption by Sector, ed. http://www.eia.gov/totalenergy/data/annual/index.cfm. 2014.

[3] Wan KW, Li HWL, Lam D, *et al*. Future trends of building heating and cooling loads and energy consumption in different climates. *Build Environ* 2011;**46**:223–34.

[4] Pacheco R, Ordóñez J, Martínez G. Energy efficient design of building: a review. *Renew Sust Energ Rev* 2012;**16**:3559–73.

[5] Su W, Darkwa J, Kokogiannakis G. Development of microencapsulated phase change material for solar thermal energy storage. *Appl Therm Eng* 2017;**112**:1205–12.

[6] Hilmarsson JG. Double Skin Facade, Construction Architect. International Line, 2008, Vol. Class 7-J, 10–13.

[7] Jiru TE, Haghighat F. Modeling ventilated double skin façade – a zonal approach. *Energy Build* 2008;**40**:1567–76.

[8] Iyi D, Hasan R, Penlington R, *et al*. Double skin façade: modelling technique and influence of venetian blinds on the airflow and heat transfer. *Appl Therm Eng* 2014;**71**:219–29.

[9] Høseggen R, Wachenfeldt BJ, Hanssen SO. Building simulation as an assisting tool in decision making Case study: with or without a double-skin facade? *Energy Build* 2008;**40**:821–7.

[10] Saber S. Energy efficiency and thermal comfort influences of alternatives of SSF and DSF in tropical bungalow house. *Int J Phys Sci* 2012;**7**:15–23.

[11] Rovers C. Natural ventilation as a means to reduce the energy consumption of the new UN HQS of Sustainability. A thesis in the light of SADD Graduation Studio A+BT Building Technology, TU Delft, 2011.

[12] Jun H. Numerical and experimental analysis of heat control and airflow in double-skin facade with integrated amorphous silicon PV cells. A thesis submitted in partial fulfilment of the requirements for the degree of Doctor of Philosophy, 2009.
[13] Yuan JZ, Zhu Y, Lin B. A lumped model of double skin facade with cavity shading. Proceedings: Building Simulation, 2007.
[14] Tanimoto J, Kimura K. Simulation study on an air flow window system with an integrated roll screen. *Energy Build* 1997;**26**:317–25.
[15] Saelens D, Roels S, Hens H. The inlet temperature as a boundary condition for multiple-skin facade modelling. *Energy Build* 2004;**36**:825–35.
[16] Tascon MH. Experimental and Computational Evaluation of Thermal Performance and Overheating in Double Skin Facades. A thesis submitted in partial fulfilment of the requirements for the degree of Doctor of Philosophy, University of Nottingham, 2008.
[17] Jager W. Double Skin Facades – Sustainable Concepts. Presentation of Hydro for Syd Bygg, 2003, Malmo, Sweden.
[18] Wigginton M. Intelligent Glass Facades by Andrea Compagno 4th edition Birkhäuser, Basel, 1999 160 pp., arq: Architectural Research Quarterly, 2008, Vol. 3.
[19] Zeng Z, Li X, Li C, *et al*. Modeling ventilation in naturally ventilated double-skin façade with a venetian blind. *Build Environ* 2012;**57**:1–6.
[20] Fallahi A, Haghighat F, Elsadi H. Energy performance assessment of double-skin façade with thermal mass. *Energy Build* 2010;**42**:1499–1509.
[21] Gracia De A, Navarro L, Castell A, *et al*. Experimental study of a ventilated facade with PCM during winter period. *Energy Build* 2013;**58**:324–32.
[22] Shen C, Li X. Solar heat gain reduction of double glazing window with cooling pipes embedded in venetian blinds by utilizing natural cooling. *Energy Build* 2016;**112**:173–83.
[23] Gracia De A, Navarro L, Castell A, *et al*. Thermal analysis of a ventilated facade with PCM for cooling applications. *Energy Build* 2013;**65**:508–15.
[24] Weinlaeder H, Koerner W, Heidenfelder M. Monitoring results of an interior sun protection system with integrated latent heat storage. *Energy Build* 2011;**43**:2468–75.
[25] Li Y, Darkwa J, Kokogiannakis G. Heat transfer analysis of an integrated double skin façade and phase change material blind system. *Build Environ* 2017;**125**:111–21.
[26] Darkwa J, Zhou T. Enhanced laminated composite phase change material for energy storage. *Energy Convers Manag* 2011;**52**:810–5.